MEASURING THE SURFACE RUGGEDNESS OF ICE-BEARING CRATERS ON MERCURY. Ariel N. Deutsch[1], Jennifer L. Heldmann[1], Anthony Colaprete[1], Richard C. Elphic[1], and Kevin M. Cannon[2], [1]NASA Ames Research Center, Mountain View, CA 94035, USA (adeutsch@usra.edu), [2]Colorado School of Mines, Golden, CO 80401, USA.

Introduction: Ice deposits were first observed at Mercury's polar regions from Earth-based radar [1–3]. Subsequent observations using the Mercury Surface, Space ENvironment, GEochemistry, and Ranging (MESSENGER) spacecraft revealed that these highly-reflective materials are cold-trapped within permanently shadowed regions [3, 4], where temperatures are sufficiently cold to sustain water ice and other volatiles [5, 6]. Enhanced neutron suppression is consistent with water ice as the primary constituent of the deposits [7], and the anomalously high reflectance of the most poleward ice deposits suggests that water ice is exposed directly at the surface [8, 9]. At lower, warmer latitudes, polar deposits have distinctly low reflectance [8, 10], where water ice is covered by a thin layer of frozen, likely organic-rich volatiles [5, 11]. Such low-reflectance surfaces correspond to maximum surface temperatures of 250–350 K and show a close spatial correlation to the surface stability boundary of coronene ($C_{24}H_{12}$) [12], although their composition has yet to be measured.

The polar deposits appear to be geologically young, due to their distinct reflectance and sharp geologic contacts [8, 10]. Crater density statistics [13] and regolith gardening and surface modification models [7, 14, 15] all suggest that the polar deposits were emplaced (or refreshed) within the last 50–200 Myr. Analyzing the surface texture of the polar deposits provides an interesting opportunity to study relatively recent surface modification on Mercury, given that surface texture evolves with time due to impact bombardment [e.g., 16, 17].

Here we analyze the surface texture of ice-bearing craters on Mercury, investigating the extent to which surface ruggedness varies between polar deposits and their host craters. Quantifying the surface texture within ice-bearing craters, and particularly across polar deposit boundaries, can help provide insight into the exposure age of the ices, and inform regolith gardening and surface evolution models.

Methods: We calculate surface ruggedness for 8 north polar craters, selected due to the availability of new high-resolution DEMs (pixel resolutions between 24 and 51 m) [12]. Ruggedness is calculated from standard deviation filtering of a 3×3 cell moving window. It is defined with a Terrain Ruggedness Index (TRI): the mean difference in elevation between a cell (i.e., a DEM pixel) and all directly adjacent cells [18]. Because surface ruggedness can be sensitive to slope, in addition to surface texture, we evaluate ruggedness values only for crater floors with slopes <10°. We compare the surface ruggedness within each crater to the crater's maximum surface temperatures, and to water-ice and coronene stability depths presented by Hamill et al. [12].

Results: *Surface ruggedness and temperature.* We note three general characteristics from our comparison between surface ruggedness and temperature (**Fig. 1**): (1) Ruggedness is relatively consistent across any given polar deposit. (2) Ruggedness increases at higher temperatures, on portions of crater floors where polar deposits are absent. (3) There is a distinct decrease in ruggedness (i.e., a smoothing) around a maximum surface temperature of ~350–400 K.

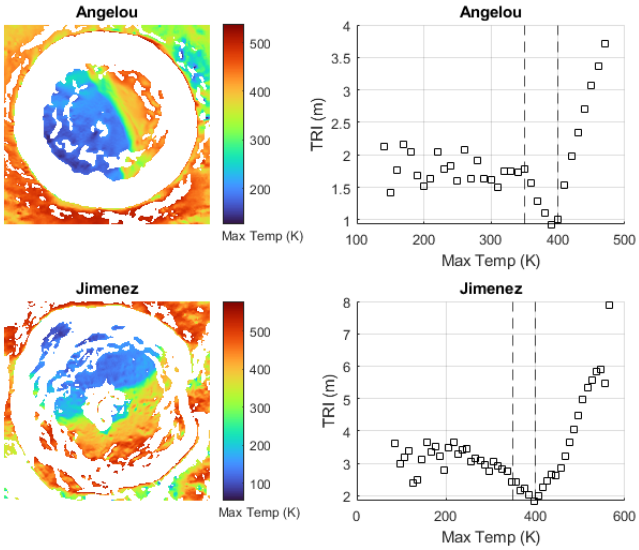

Fig. 1. (*left*) Maximum surface temperatures of Angelou (80.3°N, 293.3°E; 18.0-km diameter) and Jimenez (81.8°N, 207.7°E; 27 km). Surfaces with slopes ≥10° are masked in white. (*right*) The mean ruggedness indices of each crater's interior are plotted with respect to maximum surface temperature in 10-K increments.

Surface ruggedness and ice stability. We find that surface ruggedness is lower (i.e., smoother) where coronene is predicted to be stable at the surface and higher (i.e., rougher) where coronene is not stable at the surface (**Fig. 2**). There is typically a distinct increase in ruggedness where coronene is no longer predicted to be stable at the surface (stability depth = 0, [12]).

Surface ruggedness does not show any distinct increase where water ice is not predicted to be stable at the surface (**Fig. 2**). Although water ice is the primary constituent of the investigated polar deposits [e.g., 1–10], it is not the primary constituent of their low-reflectance surfaces [5–8]. Thus, it is unsurprising that the surface textures of these 8 polar deposits are instead strongly correlated with the surface stability depths of coronene, a simple representative for the family of complex organic materials that are expected to comprise these low-reflectance surfaces [12].

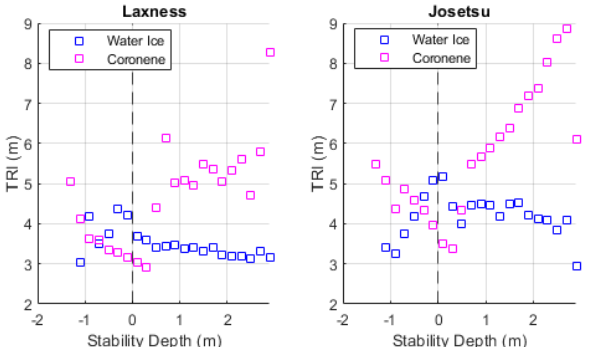

Fig. 2. The mean ruggedness indices are plotted with respect to the surface stability depths of coronene (pink) and water ice (blue) in 20-cm increments for (*left*) Laxness (83.3°N, 310.0°E) and (*right*) Josetsu (83.6°N, 225.6°E). Note: negative "Stability Depth" values indicate surface stability.

Observations at polar deposit boundaries. At each crater, there is a decrease in ruggedness beginning around 350 K (**Fig. 1**), corresponding to the maximum surface temperature where the low-reflectance polar deposits extend [12]. It is possible that this decrease is related to a smoothing effect at the polar deposit boundaries. The distinctly smooth boundary is more apparent is some craters than others (**Fig. 3**), although all craters appear to host a polar deposit (Max Temp <350 K) that is smoother than its typical floor surface (Max Temp >400 K).

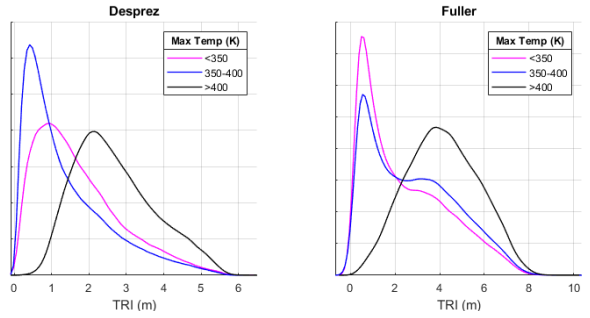

Fig. 3. The distribution of ruggedness values within (*left*) Desprez (81.1°N, 258.7°E) and (*right*) Fuller (82.6°N, 317.4°E). Surfaces where maximum temperatures are <350 K are pink, 350–400 K blue, and >400 K black.

Implications for space-weathering: The relatively smooth surfaces of the polar deposits are likely related to their young ages, as well as material property differences between ice and regolith. The physical texture of the ice provides an important record of how it has been modified by impact bombardment and regolith overturn [14, 15, 19]. Thus, the measurements of surface ruggedness presented here could be used in future surface evolution models to place constraints on the age and thickness of the low-reflectance materials.

Furthermore, the various space weathering processes operating at Mercury [19] affect the durability of volatiles as a sustainable resource for future exploration, as these processes drive modifications in volatile distribution and abundance. Therefore, understanding how relatively young ices on Mercury are modified over time is also of interest to the science and exploration of the Moon and Mars.

Conclusions: Polar deposits on Mercury appear to have a relatively smooth surface texture, distinct from the rougher surface textures of their host craters. The surface textures of Mercury's polar deposits have important implications for the weathering history and surface modification of the volatile deposits. Future measurements of polar deposit topography [20] and temperature [21] with BepiColombo will help expand our analysis to Mercury's high-latitude exposed water-ice surfaces, providing an interesting comparison of the surface textures between low-reflectance and high-reflectance polar deposits.

Acknowledgments: A.N.D. was supported by an appointment to the NASA Postdoctoral Program at Ames Research Center, administered by USRA.

References: [1] Slade M. A. et al. (1992) *Science, 258,* 635–640. [2] Harmon J. K. et al. (2011) *Icarus, 211,* 37–50. [3] Chabot N. L. et al. (2018) *JGRP, 123,* 666–681. [4] Deutsch A. N. et al. (2016) *Icarus, 280,* 158–171. [5] Zhang J. A. & Paige D. A. (2009) *GRL, 36,* L16209. [6] Paige D. A. et al. (2013) *Science, 339,* 300–303. [7] Lawrence D. J. et al. (2013) *Science, 339,* 292–296. [8] Neumann G. A. et al. (2013) *Science, 339,* 296–300. [9] Deutsch A. N. et al. (2017) *GRL, 44,* 9233–9241. [10] Chabot N. L. et al. (2014) *Geology, 42,* 1051–1054. [11] Delitsky M. L. et al. (2017) *Icarus, 281,* 19–31. [12] Hamill C. D. et al. (2020) *PSJ, 1,* 1–57. [13] Deutsch A. N. et al. (2019) *EPSL, 520,* 26–33. [14] Crider D. H. & Killen R.M. (2005*) GRL, 32,* L12201. [15] Costello E. S. et al. (2020) *JGRP, 125,* e2019JE006172. [16] Fassett C. et al. (2017) *AGU,* #P24C-01. [17] Wang J. et al. (2020) *JGRP, 125,* e2019JE006091. [18] Riley S. J. et al. (1999) *IJS, 5,* 23–27. [19] Domingue D.L. et al. (2014) *SSR, 181,* 121–214. [21] Thomas N. et al. (2007) *PSS, 55,* 1398–1413. [22] Hiesinger H. et al. (2010) *PSS, 58,* 144–165.